

Frontal and temporal coding dynamics in successive steps of complex behavior

Highlights

- Monkeys learn, retrieve, and select target objects
- Multi-electrode recordings compare activity in frontal and temporal cortex
- Strongest encoding of all task features is found on the inferior frontal convexity
- Information flows from ventral to dorsal frontal cortex

Authors

Mikiko Kadohisa, Makoto Kusunoki, Daniel J. Mitchell, Cheshta Bhatia, Mark J. Buckley, John Duncan

Correspondence

john.duncan@mrc-cbu.cam.ac.uk

In brief

Specific regions of the human brain play a domain-general role in cognitive control. In macaques, we find similar domain-general properties in ventrolateral frontal cortex (vIPFC). In complex behavior, vIPFC encodes task features earlier and more strongly than other frontal and temporal regions, with a stronger causal role in network activity.



Article

Frontal and temporal coding dynamics in successive steps of complex behavior

Mikiko Kadohisa,^{1,2} Makoto Kusunoki,^{1,2} Daniel J. Mitchell,¹ Cheshta Bhatia,³ Mark J. Buckley,² and John Duncan^{1,2,4,*}

¹MRC Cognition and Brain Sciences Unit, University of Cambridge, 15 Chaucer Road, Cambridge CB2 7EF, UK

²Department of Experimental Psychology, University of Oxford, Anna Watts Building, Radcliffe Observatory Quarter, Woodstock Road, Oxford OX2 6GG, UK

³Department of Organismic and Evolutionary Biology, Harvard University, 26 Oxford St, Cambridge, MA 02138, USA

⁴Lead contact

*Correspondence: john.duncan@mrc-cbu.cam.ac.uk

<https://doi.org/10.1016/j.neuron.2022.11.004>

SUMMARY

Ventrolateral prefrontal cortex (vlPFC), dorsolateral prefrontal cortex (dlPFC), and temporal cortex (TE) all contribute to visual decision-making. Accumulating evidence suggests that vlPFC may play a central role in multiple cognitive operations, perhaps resembling domain-general regions of the human frontal lobe. We trained monkeys in a task calling for learning, retrieval, and spatial selection of rewarded target objects. Recordings of neural activity covered large areas of vlPFC, dlPFC, and TE. Results suggested a central role for vlPFC in each cognitive operation with strong coding of each task feature, while only location was strongly coded in dlPFC and current object identity in TE. During target selection, target location was communicated first from vlPFC to dlPFC, followed by extensive mutual support. In vlPFC, stimulus identities were independently coded in different task operations. The results suggest a central role for the inferior frontal convexity in controlling successive operations of a complex, multi-step task.

INTRODUCTION

In the monkey brain, ventrolateral prefrontal cortex (vlPFC), dorsolateral prefrontal cortex (dlPFC), and temporal cortex (TE) all contribute to object-based decision-making. Strong connections between TE and vlPFC,¹ and between different frontal regions,² provide an anatomical basis for collaboration and information exchange. Much is uncertain, however, concerning the roles of different regions and how they interact.

An extensive literature has compared the neurophysiological properties of vlPFC and dlPFC. In line with strong connectivity from TE to vlPFC, and from parietal cortex to dlPFC, one influential proposal has been that vlPFC is specialized for processing objects, and dlPFC for processing locations and/or spatially directed actions (e.g., Ó Scalaidhe et al.,³ Ó Scalaidhe et al.,⁴ and Passingham and Wise⁵). In many tasks, however, both object and location information are widely spread across both vlPFC and dlPFC (e.g., Rao et al.⁶ and Rainer et al.⁷), with both regions, for example, acquiring selective location responses as the time for a movement approaches.⁸ Other evidence suggests that vlPFC may be especially central to the widespread regulation of behavior. When location memory is central to task performance, several studies have found stronger location codes in vlPFC than in dlPFC (see Cavanagh et al.,⁹ Kennerley and Wallis,¹⁰ and Markowitz et al.,¹¹ for an exception with both object and location coding stronger in dlPFC, see Meyers et al.¹²). Microstimulation of vlPFC produces widespread activation of re-

gions in the frontal cortex, parietal cortex and TE.¹³ In mixed object and location tasks, gamma power carries both object and location signals more strongly in vlPFC than in dlPFC.¹⁴ Whole-brain functional connectivity of vlPFC, assessed with fMRI, covers extensive regions of parietal, cingulate, TE, and insular cortex, resembling the extensive cognitive control network known in the human brain.^{15,16} Connectivity to multiple brain networks suggests a broad role as an attentional hub.¹⁷ In a comprehensive analysis of the neurophysiological, neuropsychological, and imaging literature, Passingham and Wise⁵ link vlPFC to many higher-order aspects of cognition, including goal setting, rule selection, and top-down control of other brain regions.

Disconnection studies confirm the importance of communication between frontal cortex and TE in a variety of object-based tasks.^{18,19} Neurophysiological studies have compared neural properties in frontal cortex and TE. Often, the nature of the monkey's task modulates neural responses in both areas but more strongly in frontal cortex. When monkeys must sort objects into behavioral categories, for example, both frontal and temporal cells show stronger discrimination between than within categories, but this happens earlier²⁰ and more strongly²¹ in frontal cortex. Responses of frontal cells also change more substantially between task and passive viewing.²⁰ In advance of a visual search array, target identity is encoded much more strongly in vlPFC than in TE, and search is substantially disrupted by local vlPFC deactivation.²² In vlPFC, object representations are



more dynamic than in TE, with poor cross-generalization between different task periods.²³

For a comprehensive comparison of neural coding in vIPFC, dIPFC, and TE, here we examined the acquisition, retrieval, and use of object information. Extending a task previously developed by Kadohisa et al.,²⁴ animals first learned that target objects were indicated by two different instruction cues, then on later trials, used cues to select target objects from a search display. We recorded activity simultaneously across large parts of vIPFC, dIPFC, and TE. On the lateral frontal surface, for clear separation of vIPFC and dIPFC, we excluded recordings within the principal sulcus (PS), focusing on dorsal and ventral convexities. The vIPFC showed involvement in all parts of the task: during learning/consolidation of the cue-object association, there was sustained coding of both cue and object; during cue-based retrieval, vIPFC was the only region to show a retrieved code of the target object; during search, the vIPFC coded target location soonest and most strongly. In all these cases, information coding was widely distributed across the inferior convexity, and for all task features, coding was notably stronger on the convexity than within either bank of the PS. In contrast, coding in the dIPFC was almost entirely restricted to target location, and even location coding was weak in comparison with vIPFC. Measures of communication between regions suggested that target location was transmitted first from vIPFC to dIPFC, followed by an extended period of mutual support. At each stage of the task, TE showed predominantly sensory responses. The results trace the distinct contributions of frontal cortex and TE to complex object- and space-based cognition. In particular, they show the broad role of the vIPFC, resembling domain-general control regions known in the human frontal cortex.^{16,25}

RESULTS

The monkey's task is illustrated in Figure 1A. In each recording session, the animal worked through a series of problems, each consisting of four cycles of trials. On each trial, six objects were presented in a circular array. The animal awaited a go cue, then selected one object by making a saccade to its location and holding fixation until feedback and (for a correct trial) reward. Across the whole study, a fixed, total set of eight objects was divided into two sets of four, associated with different color cues (four green and four yellow; Figure 1A inset). Each problem used just six objects, three from each set (see below), with all six included in each array. To ensure selection based on object identity rather than position, these six objects were randomly posi-

tioned in each array. The animal used the first cycle of the problem to learn two targets, one from each color set, then was able to re-select these same targets in cycles 2–4 to obtain further rewards.

Learning in cycle 1 called for a sequence of 2...n trials. On each trial, the animal made a selection, resulting in reward for targets and nonreward otherwise. The cycle continued until both targets had been discovered. No color cues were given in cycle 1, so that the two targets could be discovered in either order. Each target was rewarded only once; after the first target had been discovered, the animal continued to search for the second, with revisits to the first not rewarded again. In later cycles, a green or yellow cue at the start of each trial indicated which of the two targets the animal should select. Again revisits within a cycle were not allowed; after the first target had been selected, its cue did not reappear. Again, the cycle was completed once both targets had been cued and selected. Optimally, therefore, cycles 2–4 consisted of just two trials each, one for each cue and its associated target. After four cycles, the animal received signals to begin a new problem (see STAR Methods), and to encourage switching, the two objects just serving as targets were removed from the stimulus set and replaced with the two previously held out. The animal then moved on to the search for new targets in cycle 1 of the next problem.

Behavioral data for each animal are shown in Figure 1B. In cycle 1, necessarily, there were many selections of nontarget objects, while the animal found targets by trial and error. Performance then rapidly improved over cycles 2–4, with the great majority of errors being selection of an incorrect object from the cued set. Thus, animals correctly used the cues to constrain their choices but were not always immediately successful in learning which object was a target within each set. All other types of errors, including revisits, were rare throughout.

Recordings were made with semi-chronic arrays implanted in lateral frontal cortex and TE (Figure 1C). Within each array, electrodes were independently movable between recording sessions, allowing us to record different neural ensembles on different days (see STAR Methods). One 96-channel array targeted extensive regions of vIPFC and dIPFC. Based on MRI and post-mortem histology, we selected neurons recorded on the convexities of vIPFC (areas 45a, 12l, and 12r²⁶) and dIPFC (areas 46, 9, and 8). A second 32-channel array targeted the ventral surface of the TE (area TE, including TEad, TEav, TEpd, and TEpv). In total, we recorded 1,252 neurons from vIPFC (933 from animal A; 319 from animal B), 1,545 neurons from dIPFC (1,218 from animal A; 327 from animal B), and 372 neurons

of soft food reward. Saccade to other objects brought negative feedback (red square) and no reward. Problems were organized in four cycles of trials, each problem having a new pair of targets. In the first cycle, monkeys worked through a series of 2...n trials until both targets had been discovered. On each subsequent cycle, each target was rewarded once, the cycle terminating after both had been selected. Optimally, therefore, each of cycles 2–4 consisted of just two trials. The eight objects used in the experiment (fixed across sessions) were divided into two sets of four, associated with green and yellow cue stimuli, respectively (see inset). In cycle 1 there were no cues, so that monkeys could learn their two targets in either order. In cycles 2–4, each trial began with a color cue, indicating which of the two targets should be selected. In all cycles, the positive feedback signal following target selection was a square of the appropriate cue color, replacing the selected target in the array. Note that, for each problem, just six objects were used (see main text), randomly arranged in each array.

(B) Behavioral data.

(C) Recording locations. For frontal recordings, the location of each electrode is shown by a red dot. For TE, just a subset of electrodes are shown on a representative coronal brain slice; in total, 32 electrodes targeted this region. sAS, superior arcuate sulcus; iAS, inferior arcuate sulcus; PS, principal sulcus; LF, lateral fissure; STS, superior temporal sulcus.

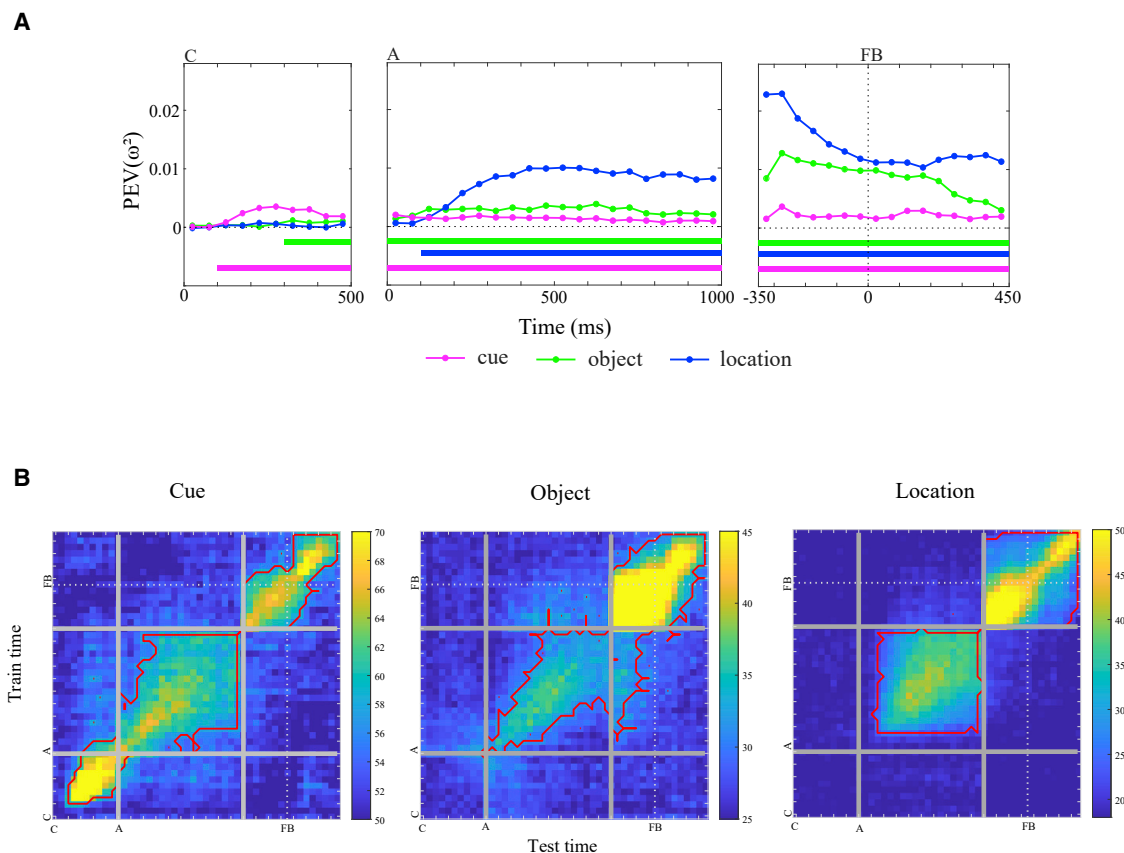


Figure 2. Coding of cue, object, and location in the vPFC

(A) Mean values of percentage explained variance for each factor, averaged across all vPFC cells ($n = 1,252$). Left panel: cue period (C, cue onset). Middle panel: array period (A, array onset). Right panel: feedback period (FB, feedback onset). Bars at bottom show periods of significant coding for each factor (see STAR Methods).

(B) Temporal cross-generalization for coding of cue (left), object (middle), and location (right). Data are percentage of correct classifications (see STAR Methods); chance = 50, 25, and 16.7 for cue, object, and location, respectively. Matching (A), each panel is split into three sections, 0–500 ms from cue onset (C), 0–1,000 ms from array onset (A), and –350 to +450 ms from feedback onset (FB). Check marks on axes at 100-ms intervals. Red outlines indicate periods of above-chance classification accuracy (see STAR Methods).

See also Figures S1–S5 and S8.

from TE (61 from animal A; 311 from animal B). For all analyses, we used just correct trials, i.e., selections of the rewarded target. Except where noted, we used data just from cycles 2 to 4, as there were no cues, and targets were unknown in cycle 1.

All task-relevant information is robustly coded in the vPFC

For the first set of analyses, we focused on the vPFC. For each neuron, spike rates were examined by ANOVA with factors cue, object, and location. Given different object sets for the two cues, we note that an effect of cue can equivalently be considered an effect of set. The object factor was then nested within cue, capturing variance between the four objects within each set. ANOVAs were conducted on spike rates in each 50 ms window, tiling the periods 0–500 ms from cue onset, 0–1,000 ms from array onset, and –350 to +450 ms from feedback onset. For each analysis window, across all recorded cells in the vPFC, we calculated a mean percentage of explained variance (PEV)

for each of the factors cue, object, and location. Time courses of these PEV values are shown in Figure 2A.

In the cue period (Figure 2A, left), the animal was able to use cue information to retrieve the target object to be selected on the current trial (Figure 1A, bottom left). Cue information became significant in the window 100–150 ms after cue onset, peaked between 200 and 300 ms, and then began to decline. Around 300 ms from cue onset, a significant effect of object appeared, indicating retrieval of the specific target object to be selected in the current problem. PEV for location remained at zero throughout the cue period, as required since target location was unpredictable.

In the array period (Figure 2A, middle), the cue remained on screen (Figure 1A, bottom), and the target object could now be localized in the array, matching many neurophysiological studies of visual search.^{22,27,28} Cue information remained significant throughout this period, at much the same reduced level seen at the end of the cue period. Object information rose to a maximum

level in the window 100–150 ms from array onset, then remaining approximately constant for the remainder of the period. Correspondingly, location information first became significant in the period 100–150 ms from array onset, increasing to a maximum around 300–500 ms and thereafter remaining high.

With the go signal and saccade to the selected object, the cue disappeared from the array, and the animal awaited the feedback signal (Figure 1A, bottom). On a correct trial, the feedback consisted of return of the cue at the selected location, confirming that the correct target had been selected (Figure 1A, bottom). As this period of the trial served to inform and/or consolidate the rules of the current problem, we broadly term it “acquisition.” In incorrect trials (not analyzed), the feedback signal was red. Following feedback, on correct trials, the animal continued to hold fixation until delivery of reward, a minimum of 450 ms from feedback onset.

Prior to feedback onset (Figure 2A, right), a strong cue signal remained, though the cue itself had now been removed. This cue signal then continued to be seen until the end of the analysis period, immediately prior to reward. Object information was high in the pre-feedback period, while the animal directly gazed at the selected object. Following feedback, though the selected object had been replaced by the return of the cue, object information reduced only slowly, remaining strong up to the time of the reward. Sustained coding of both cue and object suggests a possible role in the learning/consolidation processes required at this stage of the trial. Location information was also strong in this analysis period but hard to interpret given that different target locations were associated with different visual inputs, eye positions, and planned movements after trial end.

As a second measure of information coding, instead of mean PEV, we plotted percentage of cells with significant ($p < 0.05$) effects of each task variable in each time window. Results (Figure S1) closely mirrored those for PEV (Figure 2). Figure S2 shows the responses of example cells with selectivity for each task variable in each task phase. To select cells, we repeated ANOVAs using larger time windows (for cue period, 200–500 ms post cue onset; for array period, 500–1,000 ms from array onset; for feedback period, 0–450 ms from feedback onset), and among cells with a significant effect of a task variable, chose a cell with close to the median PEV. The results show the usual mixture of highly idiosyncratic responses in prefrontal neurons, with different activities and different selectivities across different phases of the trial.

As different cues were associated with different object sets, we asked whether some significant cue coding could be traced to simple object coding. A neuron that responded strongly to just one of the eight objects, for example, would also show an average stronger response to one of the two cues. To address this question, we asked whether neural responses were more similar for objects from the same set, i.e., associated with the same cue, than for objects from different sets. For each neuron, and each analysis window, we calculated a cue index as

$$[d(\text{between}) - d(\text{within})]/[d(\text{between}) + d(\text{within})]$$

where $d(\text{between})$ is the mean difference in spike rate for two objects from different sets, and $d(\text{within})$ is the mean difference

for two objects from the same set. The results (Figure S3, upper row) suggest true cue coding—here measured as more similar responses for objects from the same as compared with different sets—for all analysis periods except pre-feedback, i.e., for all periods when the cue was physically present in the display.

As performance progressively improved over cycles, we wondered whether, in the feedback period, cue and object coding would be stronger in early cycles, when processes related to target learning and consolidation might be most active. To assess this, ANOVAs were repeated separately for each cycle, this time including cycle 1. Results, however, suggested little change over cycles (Figure S4A), perhaps because, even by the fourth cycle, uncertainty over the cue-target association still remained (Figure 1B). More broadly, to assess possible changes over cycles or successive trials within a cycle, we repeated ANOVAs with additional factors of cycle and position within a cycle (first or second target). In all cases, however, interactions between main task variables (cue, object, and location) and either cycle or position accounted for very small proportions of variance (Figure S4B).

vIPFC representations transform over successive task operations

Next, we considered the temporal stability of vIPFC coding for cue, object, and location. To this end, we used temporal cross-generalization analysis.^{23,29} For each time window, a part of the data from each cell was used to train classifiers for cue, object, and location. We then measured the performance of these classifiers on held-out data, repeating the analysis many times with different train-test splits and averaging the results (see STAR Methods). For object decoding, classifiers were trained and tested separately for the two object sets, and the results averaged. Results are shown in Figure 2B.

For cue (Figure 2B, left), significant coding along the diagonal (train and test at same time point) matched PEV results, with cue coding strongest during cue and post-feedback periods. Across much of the trial, classification accuracy fell with movement away from the diagonal, i.e., with increasing temporal separation between train and test. A striking finding was complete absence of cross-generalization between cue and post-feedback periods. Although cue coding was strong in both periods, and though the cue stimulus in both periods was present at fixation, independent patterns of population activity distinguished cues in these two cases. The results suggest independent patterns of vIPFC activity distinguishing cue stimuli used for different purposes—in the cue period, to retrieve the target to be selected, but in the post-feedback period, to acquire the correct cue-target association.

For object (Figure 2B, middle), coding was strongest in the pre-feedback period, when the animal maintained fixation on the selected object in the array. Corresponding to PEV, significant object coding along the diagonal was maintained into the post-feedback period, though its pattern did not cross-generalize to the pre-feedback period, when the object was physically present. In the early part of the trial, object coding was first significant around 500 ms after cue onset (Figure 2B, center, end of cue period) and was clearly established by the start

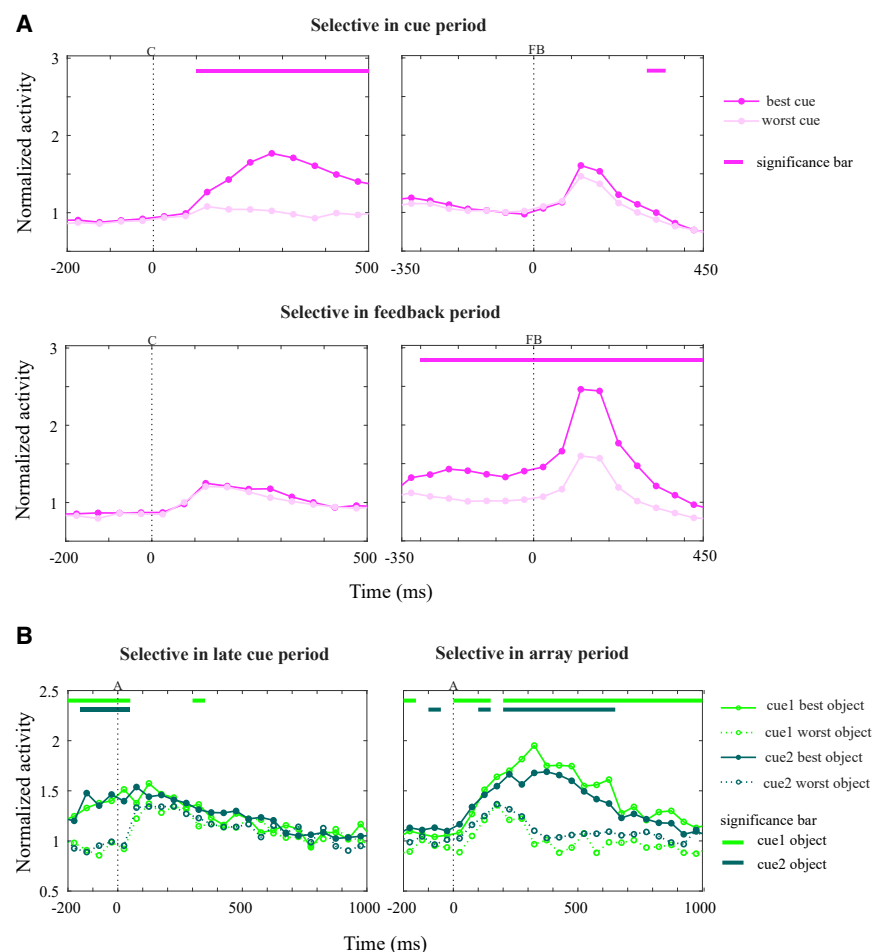


Figure 3. Temporal specificity of cue and object coding in vIPFC

(A) Mean cross-validated PSTHs (see main text and STAR Methods) for cells with significant cue coding. (top row) Cells selected and preferences defined based on cue period data; (bottom row) selection and preferences based on feedback period data. (Left panels) Activity in cue period; (right panels) activity in feedback period. Bars show significant main effects of cue across each cell sample (see STAR Methods).

(B) Cross-validated PSTHs for cells with object selectivity in late cue (left) and subsequent array (right) periods.

C, cue onset; A, array onset; and FB, feedback onset.

of the array period. Intriguingly, object coding immediately after array onset did not cross-generalize to later times. From around 200 ms post array onset, a new phase of object coding began, now cross-generalizing through much of the remaining array period. These data suggest two successive phases of object coding. The timing of the first suggests an instruction for target search, retrieved from the presented cue, while the second may reflect a stable visual description of the selected item in the array.

A related timing of events is suggested by data for location coding (Figure 2B, right). In line with PEV data, location coding arose around 200 ms following array onset and was predominantly stable, with good cross-generalization throughout the remainder of the choice period. Again these data suggest a sustained, stable description of the visual location of the selected target.

To complement this analysis, we used a second method to examine independent cue coding in cue and feedback periods. For a cross-validated assessment of cue selectivity, we split data for each neuron into two independent sets (alternate odd and even trials through the session). First, using ANOVA on the same large cue period window as before (200–500 ms post cue), we selected all cells with a main effect of cue in the data from odd trials and for each cell, defined “best” and “worst”

one half of the data were maintained in the other half (Figure 3A, top left). In contrast, cue preferences as defined in the cue period were largely unpredictable of selectivity in the feedback period (Figure 3A, top right). The same procedure using the feedback period (0–450 ms post-feedback) to select cells and define cue preferences produced equivalent results (Figure 3A, bottom). Now, within the feedback period, there was good cross-validation of cue preferences between two halves of the data (Figure 3A, bottom right), but no suggestion that cue preferences in the feedback period were mirrored by similar preferences in the cue period (Figure 3A, bottom left). In agreement with the temporal cross-generalization analysis (Figure 2B), these results confirm orthogonal cue preferences in cue and feedback periods.

A similar analysis examined the apparent change in object coding between late cue/array start and subsequent array periods. For this, we used two analysis periods, the first –150 to +50 ms and the second 300–500 ms from array onset. Now, for each half of the data, we selected cells with significant object preferences, defined best and worst objects, and examined PSTHs to these best and worst objects in the other data half. Again, the results (Figure 3B) confirmed conclusions from the temporal cross-generalization analysis (Figure 2B). Object preferences in the late cue/array start period showed good cross-validation (Figure 3B,

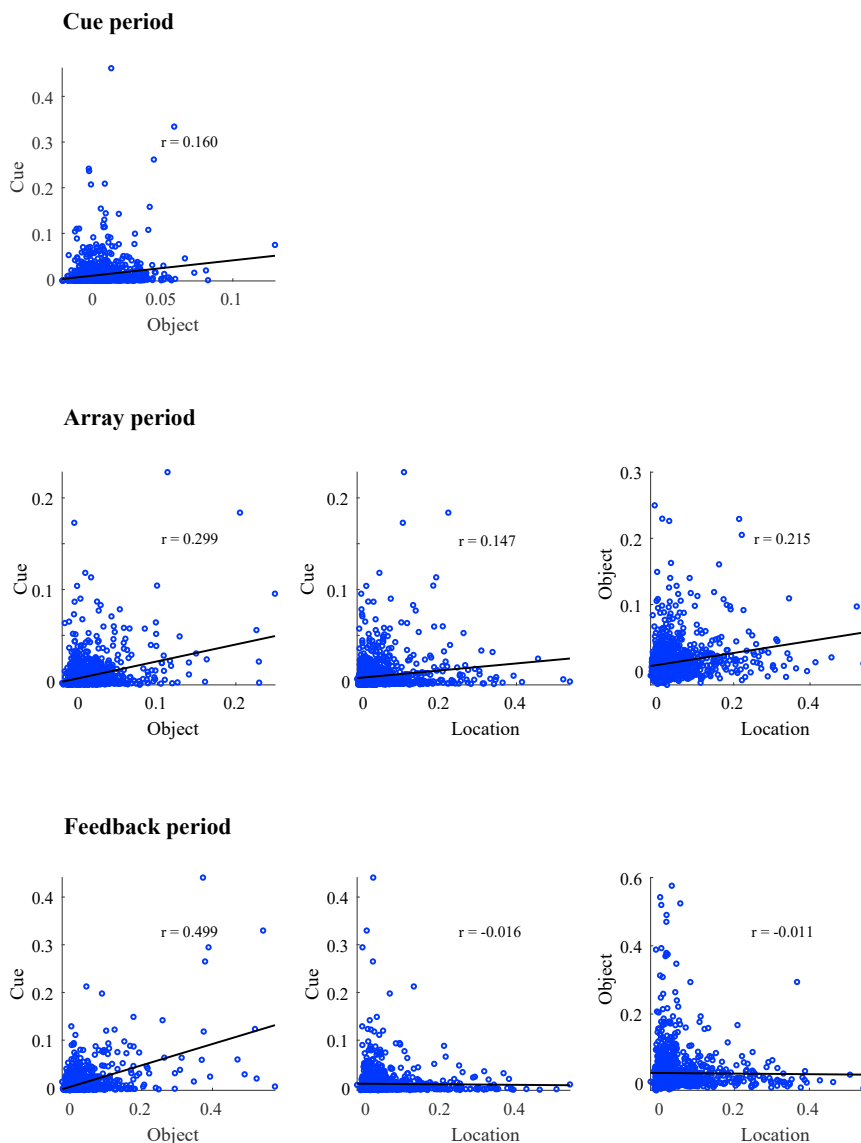


Figure 4. Multiplexed coding in vIPFC neurons

Scatterplots relating values of PEV for each pair of task features in cue (top), array (middle), and feedback (bottom) periods. Each dot shows data for one neuron.

Results are shown in Figure 4. Values of PEV for cue and object were positively correlated in all periods, while for cue-location and object-location, correlations were positive in the array period and near zero in the feedback period. These results show no tendency for different neurons to encode different task features.

Nonlinear mixed selectivity is especially important for a network's computational power, providing an explicit representation of the specific conjunction of features making up a current event.³¹ In our data, it was not possible to assess nonlinear mixed selectivity for cue and object, as a cue \times object interaction was not defined in our design. Using the same analysis windows as above, the cue \times location interaction was significant ($p < 0.05$) in 4.6%, 8.8%, and 11.7% of cells, respectively, in cue, array, and feedback periods. (Note that a chance level of 5% is expected in the cue period, before target location was known.) The object \times location interaction was significant in 5.7%, 15.7%, and 15.1% of cells.

Representational geometry in the vIPFC

For a final view of information coding in the vIPFC population, we examined representational geometry. First, we considered the geometry of cue and ob-

ject encoding. For the same cue, array, and feedback periods (200–500 ms post cue onset, 500–1,000 ms post array onset, and 0–450 ms post-feedback onset), we calculated mean spike rate for each of the eight target objects in each neuron. A two-dimensional representation of cue-object coding was then obtained using multidimensional scaling (MDS). The results (Figure 5A) matched findings from our main PEV analysis. In the cue period, there was clear separation of the two clusters of objects associated with different cues, with accompanying weak separation of objects within each cue category. Object separation then strengthened in array and feedback periods, though with remaining broad clustering into cue categories.

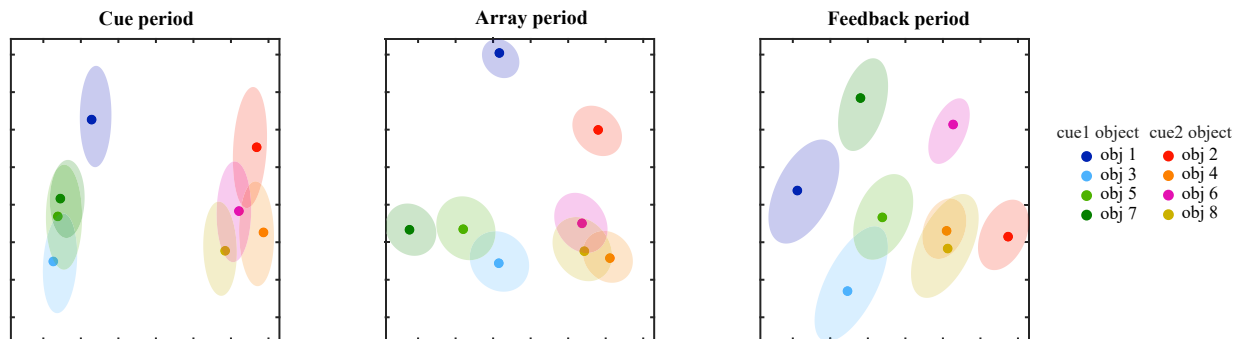
vIPFC neurons multiplex coding of cue, object, and location

A common property in frontal neurons is linear or nonlinear mixed selectivity.^{30,31} In a neuron with mixed selectivity, response rate is influenced by several stimulus or task features.

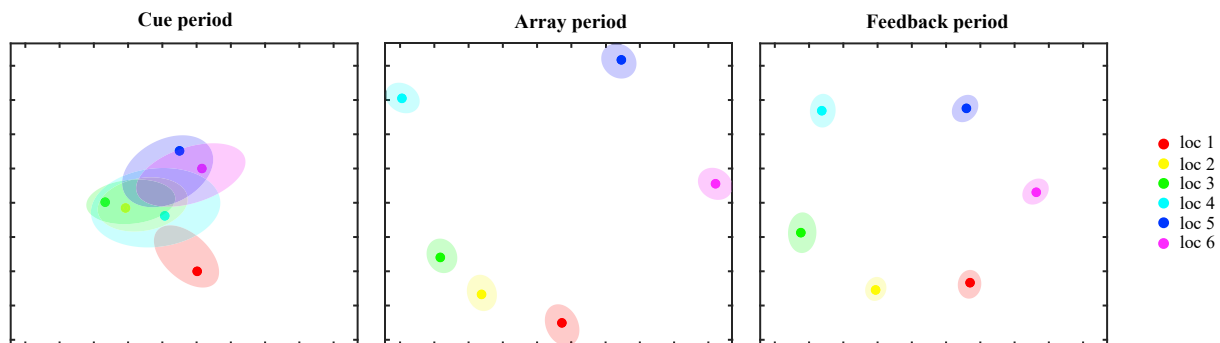
To assess simultaneous selectivity for different features, across the population of vIPFC cells, we correlated PEV values for cue, object, and location, again derived from ANOVA on long windows for each trial period (200–500 ms post cue onset, 500–1,000 ms post array onset, 0–450 ms post-feedback onset).

A second analysis instead used mean spike rates for the six different target locations (Figure 5B). As expected, clear separation of target locations emerged only in array and feedback periods, with the representational geometry matching the geometry of the array.

A



B

**Figure 5. Representational geometry in vIPFC**

Two-dimensional projection of population activity for eight objects (A) and six locations (B), obtained using multidimensional scaling. obj, object; loc, location.

Sites of selective neurons within the vIPFC

To identify where selective neurons were located within the vIPFC, we again used ANOVA on our standard time windows (200–500 ms post cue onset, 500–1,000 ms post array onset, and 0–450 ms post-feedback onset). As before, for each main effect, the significance threshold was set to $p < 0.05$, uncorrected, so that the expected chance proportion of significant cells was 5%.

Figure S5 shows the proportions of significant cells for each electrode in the recording array. For each factor and time period, significant cells were broadly distributed across the vIPFC, with no evident pattern.

Selective location coding in the dIPFC

We turned next to dIPFC and again assessed separate coding of cue, object, and location. PEV results are shown in Figure 6A, with equivalent results for vIPFC reproduced from Figure 2A for comparison. In contrast to vIPFC, there was no significant coding of cue and very weak coding of object. The latter was seen especially in the pre-feedback and immediate post-feedback periods when the selected object was fixated and immediately after it disappeared. For much of the trial, cue and object coding were significantly less strong than in vIPFC (Figure 6A, open bars).

In contrast, location coding was clear in the dIPFC, beginning in the array period and again extending through the remainder of

the trial. Following array onset, compared with vIPFC, location coding in the dIPFC followed a similar time course, but was weaker throughout. Significant location coding in the window 0–50 ms from array onset is likely a false positive ($p < 0.03$), as it is not plausible that the target could be localized so soon. Location coding was also strong in the later part of the trial, following saccade to the selected target, but again is hard to interpret given the multiple sensory and motor factors that might contribute.

Temporal cross-generalization results for location are shown in Figure 6B. In line with PEV results, coding of cue and object was weak and in this analysis nonsignificant. The dynamics of location coding resembled those of the vIPFC (Figure 2B). Again, once location coding arose in the array period, good cross-generalization across time points showed largely stable coding for the remainder of the period.

Recording sites of cells with a significant effect of location ($p < 0.05$, same time windows as before) are shown in Figure S6. As we found for vIPFC, significant cells were broadly distributed across the dIPFC, with no clear suggestion of clustering.

Sensory coding in temporal cortex

Finally, we turned to cue, object, and location coding in our smaller sample of cells from TE. At the start of the trial, cue coding became significant in the period 150–200 ms post cue onset, then as in vIPFC, remained significant for most of the remainder

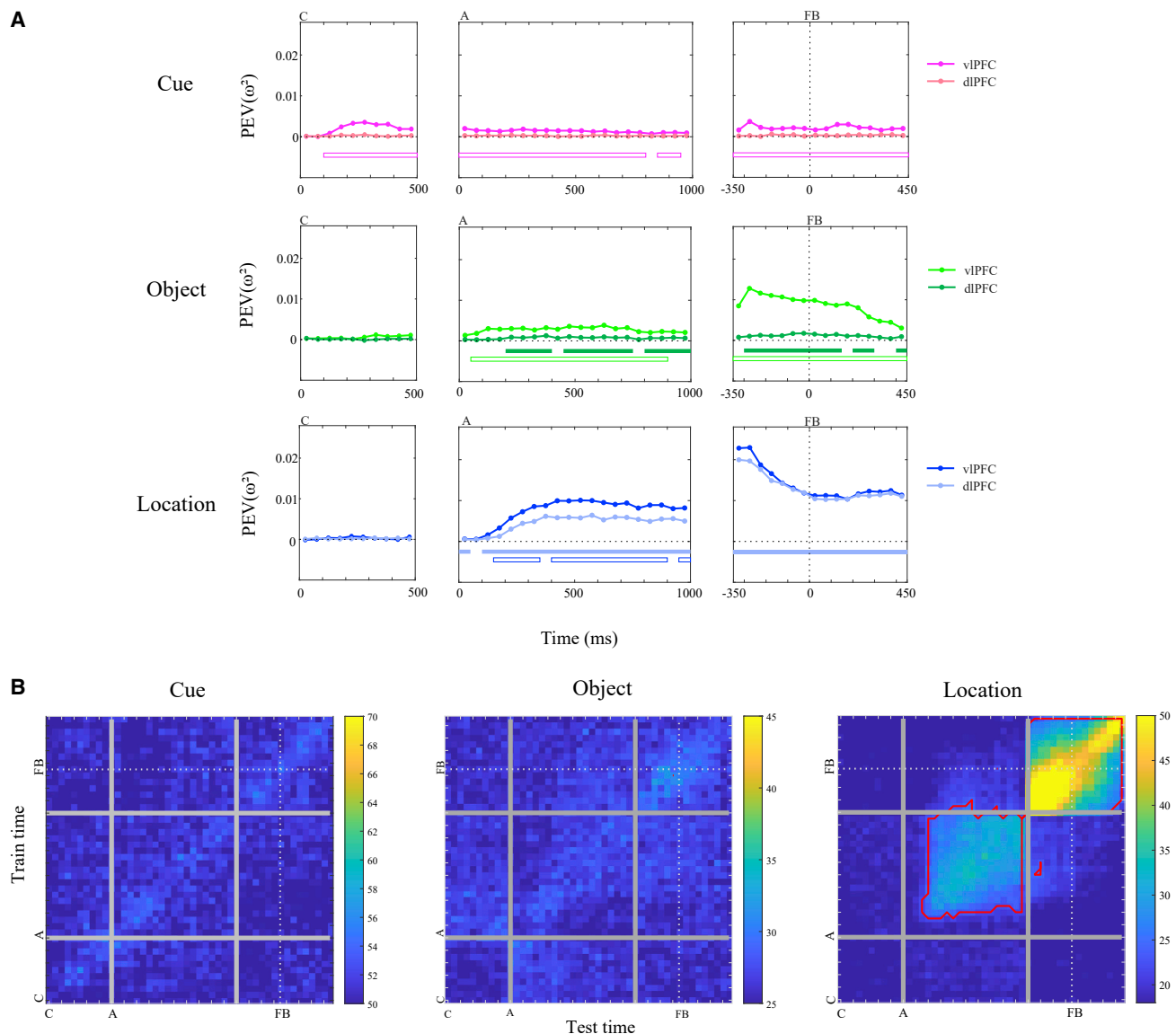


Figure 6. Coding of cue, object, and location in the dlPFC

(A) Mean values of percentage explained variance for each factor, averaged across all dIPFC cells (n = 1,545). Data for vIPFC are copied from [Figure 2A](#) for comparison. Filled bars show periods of significant coding within dIPFC; open bars show significant difference between dIPFC and vIPFC (see [STAR Methods](#)). Other conventions as [Figure 2A](#).

(B) Temporal cross-generalization. Conventions as Figure 2B.

See also [Figure S6](#).

of the cue period (Figure 7A). In contrast to vIPFC, there was no hint of a retrieved object code in this period; instead, the results suggested only a simple visual response to the cue stimulus. Cue coding remained significant throughout the array period but was accompanied by only scattered time points of object and location coding. In contrast to frontal regions, these data suggest only a weakly selective response to the chosen item in the array. In the pre-feedback period, there was now strong object coding, reflecting the usual strong temporal lobe response to the object at fixation. In contrast to vIPFC, however, object coding declined rapidly after feedback, when the foveated target was replaced

with the returning cue. At this point, instead, cue information strengthened, matching return of the cue stimulus on the screen. Again, these data are consistent with response largely driven by the visual properties of the foveal stimulus.

These conclusions are supported by temporal cross-generalization analysis (Figure 7B). In strong contrast to vIPFC, there was now some cross-generalization between cue representations at cue and post-feedback periods, in line with a simple sensory response. Matching PEV results, object coding was only strong in the pre-feedback period, with good cross-generalization throughout this period. Again matching PEV results, there

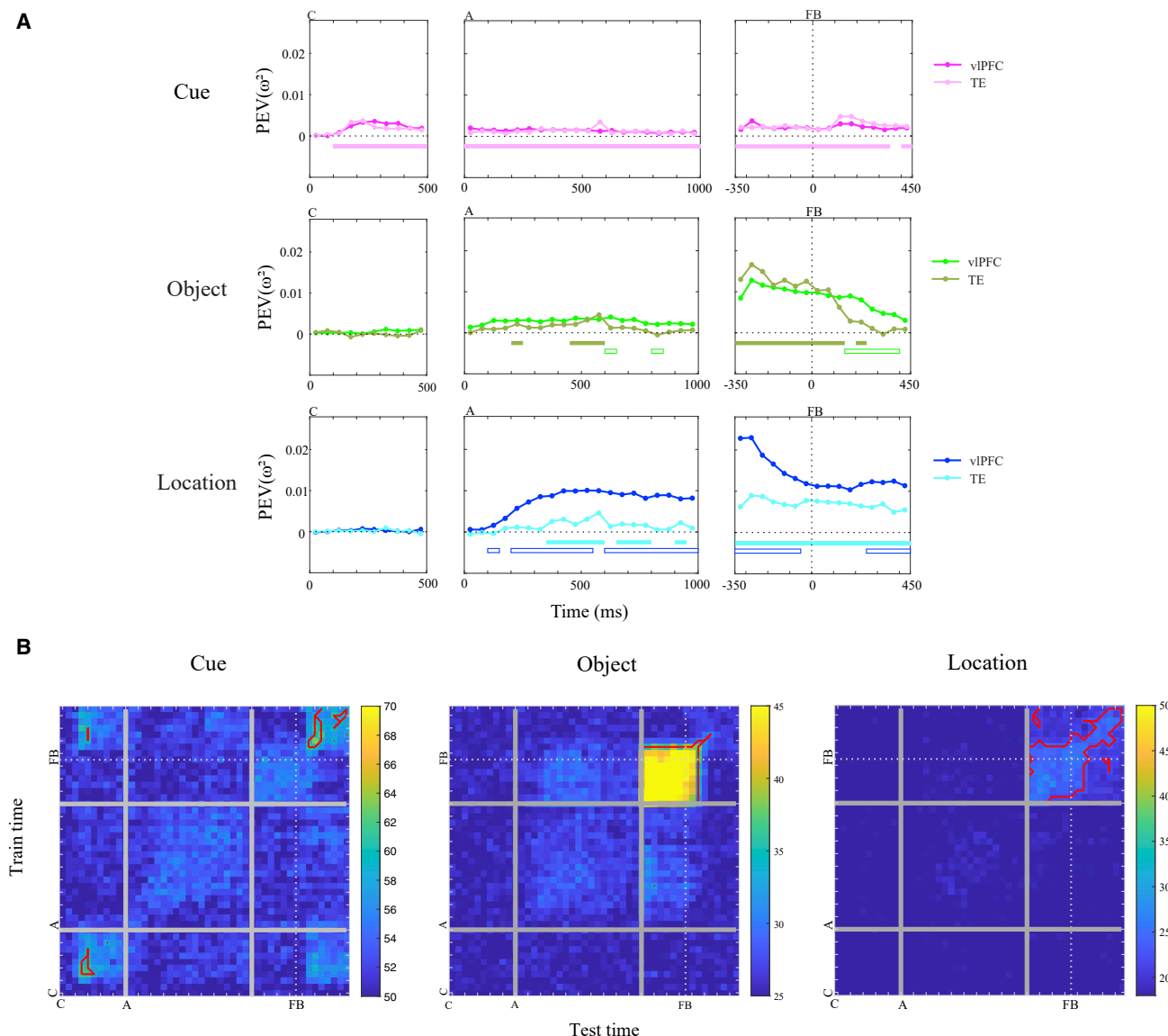


Figure 7. Coding of cue, object, and location in TE

(A) Mean values of percentage explained variance for each factor, averaged across all TE cells ($n = 372$). Filled bars show periods of significant coding within TE; open bars show significant difference between TE and vIPFC (see [STAR Methods](#)). Other conventions as [Figure 2A](#).

(B) Temporal cross-generalization. Conventions as [Figure 2B](#).

See also [Figure S7](#).

was also little hint of location coding until after the eye had moved to the target location.

As we had for vIPFC, we used a supplementary analysis of similarity within and between object sets to ask whether apparent cue coding might be traced to simple preference for individual objects in one or the other set. Again, results suggested genuine cue coding throughout the trial, except for the pre-feedback period when the cue stimulus was removed from the display ([Figure S3](#), lower row).

Recording sites of cells with a significant effects of each task feature ($p < 0.05$, same time windows as before) are shown in

[Figure S7](#). In each task period, significant cells were broadly distributed across the recording area.

Recordings within the principal sulcus

For our main analyses, as noted above, we selected neurons recorded on dorsal and ventral convexities. In addition, we recorded from 539 neurons on the dorsal bank of the PS (dPS) and 939 neurons on the ventral bank of the PS (vPS). For comparison with our major findings, PEV results for these two additional groups of neurons are shown in [Figure S8](#). For all three task features, cue, object, and location, there were multiple periods of

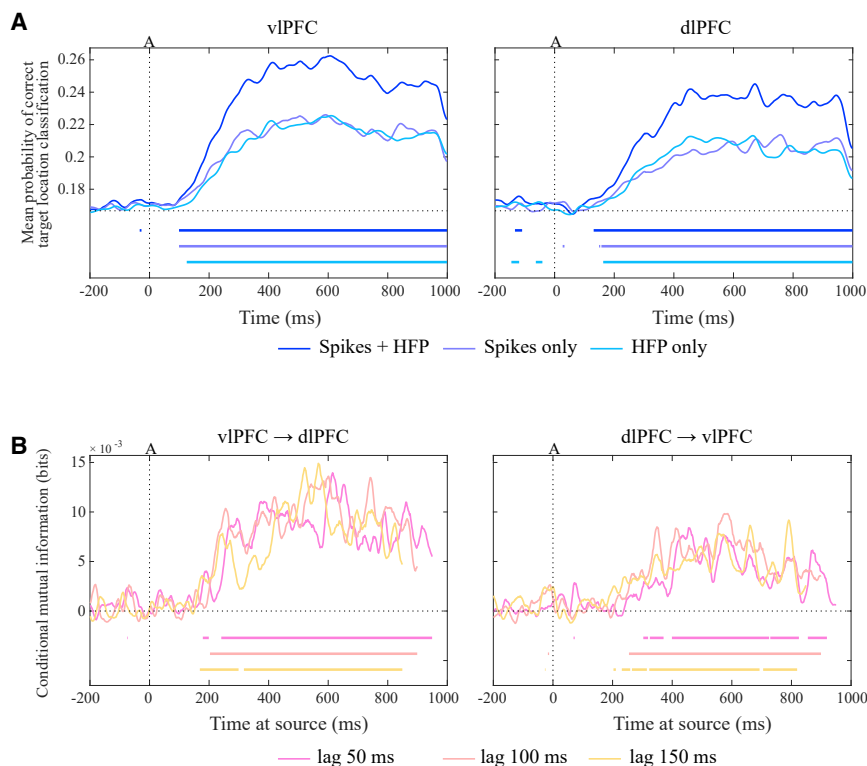


Figure 8. Communication between regions

(A) Mean single-trial estimates of correct target location in vIPFC (left) and dIPFC (right), derived from linear discriminant analysis based on spike, high frequency power (HFP), or both types of data. Data come from 16 sessions with at least 15 recorded neurons in each region. Chance = 0.167 (horizontal dotted line).

(B) Conditional mutual information between information time courses (spikes+HFP data; A, dark blue) in the direction vIPFC > dIPFC (left) and dIPFC > vIPFC (right), at lags between source and target region of 50, 100, and 150 ms. A, array onset.

stronger coding in vIPFC than in either PS region. In contrast, despite numerically stronger coding of all three features in vPS than in dPS, these differences were never significant.

Communication between regions

Finally, we wished to ask how task-relevant information is communicated between brain regions. For this purpose, we used conditional mutual information,^{32,33} a nonparametric analog to Granger causality (see STAR Methods). As an index of communication, the method asks whether the state of a source region X at time t predicts the state of a target region Y at a later time t + lag, over and above prediction from the state of Y itself at time t. Because target location was strongly coded in both vIPFC and dIPFC, we focused on transfer of location information between these two regions. As the method required robust single-trial estimates of location information in each region, we selected a set of 16 sessions with at least 15 recorded neurons in both vIPFC and dIPFC (mean of 22.2 neurons from 14.9 electrodes in vIPFC; mean 24.5 neurons from 17.0 electrodes in dIPFC). All sessions came from animal A.

On each trial, for each region, we obtained a continuous time course of location coding (Figure 8A). To obtain these time courses (see STAR Methods), we used a cross-validated linear discriminant classifier, whose output at each time point was the probability of assigning the population data to the correct target location (chance = 0.167). We used three types of classifiers, one based on instantaneous spike rate from each recorded neuron, the second based on high frequency power (HFP; 70–250 Hz) from each electrode, often used as a proxy for local neural activity, and the third based on both types of features com-

bined. The results (Figure 8A) confirmed that location coding was stronger in vIPFC than in dIPFC, in particular with a more rapid increase after array onset. As expected if both signals are informative, location was most strongly decoded in the analysis combining spikes and HFP.

Given most information in the spike+HFP time course, we selected this time course for the conditional mutual information analysis. For each time point, the classifier output for the source region was used to predict output for the target

region across a range of lags (1–200 ms), once with vIPFC as the source and dIPFC as the target, once the reverse. For each lag, the result was a time course of conditional mutual information in each direction (for three example lags, see Figure 8B). For the direction vIPFC > dIPFC, across a range of lags, the results showed conditional mutual information arising sharply beyond about 200 ms from array onset, then remaining strongly significant throughout the remainder of the array period. Conditional mutual information was also significant in the direction dIPFC > vIPFC, but in this direction it began later and was generally weaker, though still significant over an extended period. We note that, in this type of analysis, latencies and lags cannot be simply interpreted if signals are autocorrelated. For example, even if information flows from the source to target only at time t, there will be conditional mutual information at earlier times and longer lags if the source signal at time t is correlated with the source signal at earlier times. With this caveat, the data suggest that, following array onset, location information flowed first from vIPFC to dIPFC, followed by a later, extended period of mutual exchange.

DISCUSSION

Using large, semi-chronic electrode arrays, we recorded simultaneously from three brain regions—vIPFC, focusing on the inferior frontal convexity, dIPFC, and TE—during a task that required learning, retrieval, and selection of a rewarded target object. On each trial, the animal was presented with a six-object array and, on receipt of a go signal, made a saccade to one selected object and held it for positive or negative feedback. In the first cycle of

trials, animals had the opportunity to learn two target objects, bringing reward when they were selected, each associated with a different color cue. In subsequent cycles, each trial began with a cue, and the animal was rewarded for selecting the corresponding target object. We focused analysis on correct trials in cycles 2–4, after the animal's first opportunity to learn the two targets.

Results showed involvement of vIPFC at each task stage. In the cue period, coding of cue identity was followed by a retrieved code indicating the specific target object. This retrieved object code was unique to vIPFC, with no similar activity in either dIPFC or TE. Plausibly, this representation served to direct localization and selection of the target in the subsequent array, and indeed, both cue and object codes continued into the start of the array period. These results support previous findings by Bichot et al.,²² in which monkeys freely scanned a complex object array in search of a specific target. In that study, prior to array onset, target identity was more strongly represented in vIPFC than TE, and pharmacological suppression of vIPFC activity strongly impaired performance.

Around 200 ms from array onset, we found large changes in vIPFC coding. A rapid increase in location coding showed that the target was localized in the array. At approximately the same time, object coding strengthened and changed its form, reflected in little cross-generalization to earlier time points. Many cells showed conjunctive coding for object and location, reflected in a significant object \times location interaction. Both location and object codes then remained stable as the animal awaited the go signal. These sustained activities thus encoded the properties of the relevant or attended object in the visual periphery.

Yet a new set of properties emerged in vIPFC at around feedback delivery at the end of each trial. Feedback served to inform and/or consolidate the rules of the current problem, linking each cue to its associated target. In vIPFC, correspondingly, both cue and object codes were strong and sustained following feedback delivery, suggesting an extended role in rule learning. Strikingly, though cue coding was strong in both cue and post-feedback periods, during both of which the cue stimulus was present at fixation, temporal cross-generalization showed independent cue codes in these two time periods. Such results resemble previous demonstrations that the object preferences of frontal neurons dissociate at different stages of a trial (e.g., Meyers et al.,²³ Kadohisa et al.,²⁴ Sigala et al.,³⁴ and Warden and Miller³⁵). They show independent cue codes in vIPFC for cue-target learning and cued target retrieval.

Across the vIPFC population, there was much multiplexing of coding for different task features. At each stage of the trial, PEV values for cue and object were positively correlated, showing involvement of the same cells in encoding these two task features. In the array period, though not in the feedback period, PEV values for location were also positively correlated with values for cue and object. Linear and nonlinear mixed selectivity is widely known in frontal neurons, allowing single neurons to represent conjunctions of two or more task features.³¹ Neurons encoding multiple task features may contribute to an integrated vIPFC model of current events, including the current cue-target pair, and the conjunction of properties possessed by a currently attended array item.

At each trial period, cells coding for cue, object, and location were widely distributed in the vIPFC. These results show involve-

ment of the same, large area of the inferior frontal convexity across multiple task operations, including learning from feedback, cue-based retrieval, and spatial target selection.

Compared with vIPFC, quite different properties were seen in dIPFC and TE. In dIPFC, only target location was strongly coded, beginning shortly after the onset of the search array. Throughout the array period, location coding was somewhat stronger in vIPFC, contrary to the classical proposal that spatial processing is predominantly the function of dIPFC, but in line with several previous reports of stronger task-relevant spatial codes in vIPFC.^{9,10} TE, meanwhile, showed properties largely consistent with simple sensory responses. Unlike vIPFC, there was no evidence that the identity of the target object was represented in advance of the search array; though retrieved object codes have previously been demonstrated in TE,^{36,37} there was no evidence for this in our task and recording area. Even when the array appeared, and the target was selected within it, TE showed only scattered, weak periods of location and object coding. Compared with vIPFC, these data suggest less modulation of the visual response by attention to the selected target. Instead, the identity of the target object was only strongly represented after the saccade, when this object was at the fovea. In contrast to vIPFC, this strong object representation rapidly disappeared in the post-feedback period when the target object was no longer visible. Further evidence of sensory responses arose from coding of cue identity, strong and cross-generalized in cue and post-feedback periods.

Following the onset of the search array, strong representation of target identity and location in the vIPFC, with weaker, less reliable coding in dIPFC and TE, suggests that the target selection process in vIPFC may direct selection in other regions. A possible mechanism is support between congruent location representations in vIPFC and dIPFC and between congruent object representations in vIPFC and TE. This suggestion is in line with the proposal that visual attention develops through support between representations of the same object across multiple cortical and subcortical regions³⁸ and more generally, with the common proposal that frontal cortex exerts top-down control over other brain regions.^{39–41} The vIPFC may be a major source of such bias signals, at least in visual search for an object target (Bichot et al.,²² see also Passingham and Wise⁵).

These suggestions were extended by the analysis of communication between vIPFC and dIPFC using conditional mutual information. Following array onset, communication of a target location code occurred first in the direction vIPFC \rightarrow dIPFC, with the code in vIPFC at time t predicting the dIPFC code at a later time $t + \text{lag}$, over and above prediction from the time t code in dIPFC itself. This was followed by an extended period of mutual support, with the time t location code in each region predicting the code at time $t + \text{lag}$ in the other, over and above the within-region prediction. These influences appeared across a wide range of lags. The idea that mutual support leads multiple prefrontal regions to converge on a congruent coding state resembles prior findings in a target detection task with two stimuli in a visual array, one to either side of fixation.^{42,43} Early in the array period, the firing of frontal neurons in each hemisphere was dominated by the contralateral stimulus, but later, a congruent code in both hemispheres indicated target present or absent.

In a previous report,²⁴ using a simplified version of the present task, we described weak object selectivity within and to either side of the PS. The present results show stronger object coding on a large region of the inferior convexity. More broadly, though some studies suggest stronger object coding in ventrolateral than in dorsolateral frontal cortex (e.g., Ó Scalaidhe et al.,³ Ó Scalaidhe et al.,⁴ and Tang et al.⁴⁴), others find widespread object coding in both (e.g., Rao et al.⁶ and Rainer et al.⁷). Several factors could influence regional differentiation. Within one region, results may evolve through the time course of a trial, with early differentiation between frontal regions disappearing as they converge on a common final state (e.g., Cai and Padoa-Schioppa⁸ and Kusunoki et al.⁴⁵), in line with rich frontal interconnections.^{2,5} Specializations may also vary over learning. Human imaging data suggest that learning focuses frontal representations on task-relevant distinctions,⁴⁶ in line with modeling work showing that, in a recurrent neural network, learning produces increasingly focused task-relevant activity.⁴⁷

Human imaging data have repeatedly demonstrated a “cognitive control” or “multiple-demand” network, with tightly defined components in lateral frontal cortex, anterior cingulate, insula, intraparietal sulcus, and occipito-temporal border.^{16,25,48,49} Multiple-demand regions are characterized by increased activity during many different cognitive operations, strong mutual connectivity, and representations of many different kinds of information,^{16,50} suggesting a broad role in assembling cognitive operations through integration of their distributed components. In the macaque, functional connections of the vIPFC are strongly reminiscent of the human multiple-demand network.^{15,51} In our data, vIPFC moved through a series of states, encoding the contents of each successive cognition operation—cue identification, target object retrieval, target discovery, and encoding of the target’s visual properties, and finally feedback processing and learning. Task-relevant representations of both object and location arose more strongly in vIPFC than in dIPFC or TE, evolved rapidly as different cognitive operations were executed, and showed the conjunctive coding needed to integrate an operation’s elements. In line with human imaging data, these findings point to a specific region of lateral frontal cortex involved in diverse forms of cognitive control, matching the recent suggestion that vIPFC can act as an “attentional hub.”¹⁷

STAR★METHODS

Detailed methods are provided in the online version of this paper and include the following:

- **KEY RESOURCES TABLE**
- **RESOURCE AVAILABILITY**
 - Lead contact
 - Materials availability
 - Data and code availability
- **EXPERIMENTAL MODEL AND SUBJECT DETAILS**
- **METHOD DETAILS**
 - Task
 - Recordings
- **QUANTIFICATION AND STATISTICAL ANALYSIS**

SUPPLEMENTAL INFORMATION

Supplemental information can be found online at <https://doi.org/10.1016/j.neuron.2022.11.004>.

ACKNOWLEDGMENTS

This work was supported by Medical Research Council UK Program MC_UU_00030/7 and Wellcome Trust grant 101092/Z/13/Z.

AUTHOR CONTRIBUTIONS

M. Kadohisa, M. Kusunoki, M.J.B., and J.D. designed the research. M. Kadohisa and M. Kusunoki collected data. M. Kadohisa, M. Kusunoki, D.J.M., C.B., and J.D. analyzed data. J.D. and D.J.M. wrote the paper. J.D. and M.J.B. supervised the work.

DECLARATION OF INTERESTS

The authors declare no competing interests.

Received: March 1, 2022

Revised: June 21, 2022

Accepted: November 3, 2022

Published: December 5, 2022

REFERENCES

1. Ungerleider, L.G., Gaffan, D., and Pelak, V.S. (1989). Projections from inferior temporal cortex to prefrontal cortex via the uncinate fascicle in rhesus monkeys. *Exp. Brain Res.* 76, 473–484.
2. Pucak, M.L., Levitt, J.B., Lund, J.S., and Lewis, D.A. (1996). Patterns of intrinsic and associational circuitry in monkey prefrontal cortex. *J. Comp. Neurol.* 376, 614–630.
3. Ó Scalaidhe, S.P., Wilson, F.A.W., and Goldman-Rakic, P.S. (1997). Areal segregation of face-processing neurons in prefrontal cortex. *Science* 278, 1135–1138.
4. Ó Scalaidhe, S.P., Wilson, F.A.W., and Goldman-Rakic, P.S. (1999). Face-selective neurons during passive viewing and working memory performance of rhesus monkeys: evidence for intrinsic specialization of neuronal coding. *Cereb. Cortex* 9, 459–475.
5. Passingham, R.E., and Wise, S.P. (2012). *The Neurobiology of the Prefrontal Cortex: Anatomy, Evolution, and the Origin of Insight* (Oxford University Press).
6. Rao, S.C., Rainer, G., and Miller, E.K. (1997). Integration of what and where in the primate prefrontal cortex. *Science* 276, 821–824.
7. Rainer, G., Asaad, W.F., and Miller, E.K. (1998). Memory fields of neurons in the primate prefrontal cortex. *Proc. Natl. Acad. Sci. USA* 95, 15008–15013.
8. Cai, X., and Padoa-Schioppa, C. (2014). Contributions of orbitofrontal and lateral prefrontal cortices to economic choice and the good-to-action transformation. *Neuron* 81, 1140–1151.
9. Cavanagh, S.E., Towers, J.P., Wallis, J.D., Hunt, L.T., and Kennerley, S.W. (2018). Reconciling persistent and dynamic hypotheses of working memory coding in prefrontal cortex. *Nat. Commun.* 9, 3498.
10. Kennerley, S.W., and Wallis, J.D. (2009). Reward-dependent modulation of working memory in lateral prefrontal cortex. *J. Neurosci.* 29, 3259–3270.
11. Markowitz, D.A., Curtis, C.E., and Pesaran, B. (2015). Multiple component networks support working memory in prefrontal cortex. *Proc. Natl. Acad. Sci. USA* 112, 11084–11089.
12. Meyers, E.M., Qi, X.-L., and Constantinidis, C. (2012). Incorporation of new information into prefrontal cortical activity after learning working memory tasks. *Proc. Natl. Acad. Sci. USA* 109, 4651–4656.
13. Xu, R., Bichot, N.P., Takahashi, A., and Desimone, R. (2022). The cortical connectome of primate lateral prefrontal cortex. *Neuron* 110, 312–327.

14. Lundqvist, M., Rose, J., Herman, P., Brincat, S.L., Buschman, T.J., and Miller, E.K. (2016). Gamma and beta bursts underlie working memory. *Neuron* 90, 152–164.
15. Neubert, F.X., Mars, R.B., Thomas, A.G., Sallet, J., and Rushworth, M.F. (2014). Comparison of human ventral frontal cortex areas for cognitive control and language with areas in monkey frontal cortex. *Neuron* 81, 700–713.
16. Assem, M., Glasser, M.F., Van Essen, D.C., and Duncan, J. (2020). A domain-general cognitive core defined in multimodally parcellated human cortex. *Cereb. Cortex* 30, 4361–4380.
17. Trambaiolli, L.R., Peng, X., Lehman, J.F., Linn, G., Russ, B.E., Schroeder, C.E., Liu, H., and Haber, S.N. (2022). Anatomical and functional connectivity support the existence of a salience network node within the caudal ventrolateral prefrontal cortex. *eLife* 11, e76334.
18. Eacott, M.J., and Gaffan, D. (1992). Inferotemporal-frontal disconnection: the uncinate fascicle and visual associative learning in monkeys. *Eur. J. Neurosci.* 4, 1320–1332.
19. Tomita, H., Ohbayashi, M., Nakahara, K., Hasegawa, I., and Miyashita, Y. (1999). Top-down signal from prefrontal cortex in executive control of memory retrieval. *Nature* 401, 699–703.
20. McKee, J.L., Riesenhuber, M., Miller, E.K., and Freedman, D.J. (2014). Task dependence of visual and category representations in prefrontal and inferior temporal cortices. *J. Neurosci.* 34, 16065–16075.
21. Freedman, D.J., Riesenhuber, M., Poggio, T., and Miller, E.K. (2003). A comparison of primate prefrontal and inferior temporal cortices during visual categorization. *J. Neurosci.* 23, 5235–5246.
22. Bichot, N.P., Heard, M.T., DeGennaro, E.M., and Desimone, R. (2015). A source for feature-based attention in the prefrontal cortex. *Neuron* 88, 832–844.
23. Meyers, E.M., Freedman, D.J., Kreiman, G., Miller, E.K., and Poggio, T. (2008). Dynamic population coding of category information in inferior temporal and prefrontal cortex. *J. Neurophysiol.* 100, 1407–1419.
24. Kadohisa, M., Watanabe, K., Kusunoki, M., Buckley, M.J., and Duncan, J. (2020). Focused representation of successive task episodes in frontal and parietal cortex. *Cereb. Cortex* 30, 1779–1796.
25. Fedorenko, E., Duncan, J., and Kanwisher, N. (2013). Broad domain generality in focal regions of frontal and parietal cortex. *Proc. Natl. Acad. Sci. USA* 110, 16616–16621.
26. Saleem, K.S., and Logothetis, N.K. (2012). *A Combined MRI and Histology Atlas of the Rhesus Monkey Brain in Stereotaxic Coordinates*, Second Edition (Academic Press).
27. Chelazzi, L., Miller, E.K., Duncan, J., and Desimone, R. (1993). A neural basis for visual search in inferior temporal cortex. *Nature* 363, 345–347.
28. Thompson, K.G., Hanes, D.P., Bichot, N.P., and Schall, J.D. (1996). Perceptual and motor processing stages identified in the activity of macaque frontal eye field neurons during visual search. *J. Neurophysiol.* 76, 4040–4055.
29. Stokes, M.G., Kusunoki, M., Sigala, N., Nili, H., Gaffan, D., and Duncan, J. (2013). Dynamic coding for cognitive control in prefrontal cortex. *Neuron* 78, 364–375.
30. Rigotti, M., Ben Dayan Rubin, D.D., Wang, X.-J., and Fusi, S. (2010). Internal representation of task rules by recurrent dynamics: the importance of the diversity of neural responses. *Front. Comp. Neurosci.* 4, 24.
31. Rigotti, M., Barak, O., Warden, M.R., Wang, X.-J., Daw, N.D., Miller, E.K., and Fusi, S. (2013). The importance of mixed selectivity in complex cognitive tasks. *Nature* 497, 585–590.
32. Ince, R.A., van Rijsbergen, N.J., Thut, G., Rousselet, G.A., Gross, J., Panzeri, S., and Schyns, P.G. (2015). Tracing the flow of perceptual features in an algorithmic brain network. *Sci. Rep.* 5, 17681.
33. Ince, R.A., Giordano, B.L., Kayser, C., Rousselet, G.A., Gross, J., and Schyns, P.G. (2017). A statistical framework for neuroimaging data analysis based on mutual information estimated via a gaussian copula. *Hum. Brain Mapp.* 38, 1541–1573.
34. Sigala, N., Kusunoki, M., Nimmo-Smith, I., Gaffan, D., and Duncan, J. (2008). Hierarchical coding for sequential task events in the monkey prefrontal cortex. *Proc. Natl. Acad. Sci. USA* 105, 11969–11974.
35. Warden, M.R., and Miller, E.K. (2010). Task-dependent changes in short-term memory in the prefrontal cortex. *J. Neurosci.* 30, 15801–15810.
36. Sakai, K., and Miyashita, Y. (1991). Neural organization for the long-term memory of paired associates. *Nature* 354, 152–155.
37. Naya, Y., Yoshida, M., and Miyashita, Y. (2001). Backward spreading of memory-retrieval signal in the primate temporal cortex. *Science* 291, 661–664.
38. Duncan, J., Humphreys, G.W., and Ward, R. (1997). Competitive brain activity in visual attention. *Curr. Opin. Neurobiol.* 7, 255–261.
39. Norman, D., and Shallice, T. (1980). *Attention to Action: Willed and Automatic Control of Behavior* (Report No. 8006) (University of California, Center for Human Information Processing).
40. Desimone, R., and Duncan, J. (1995). Neural mechanisms of selective visual attention. *Annu. Rev. Neurosci.* 18, 193–222.
41. Miller, E.K., and Cohen, J.D. (2001). An integrative theory of prefrontal cortex function. *Annu. Rev. Neurosci.* 24, 167–202.
42. Kadohisa, M., Petrov, P., Stokes, M., Sigala, N., Buckley, M., Gaffan, D., Kusunoki, M., and Duncan, J. (2013). Dynamic construction of a coherent attentional state in a prefrontal cell population. *Neuron* 80, 235–246.
43. Erez, Y., Kadohisa, M., Petrov, P., Sigala, N., Buckley, M.J., Kusunoki, M., and Duncan, J. (2022). Integrated neural dynamics for behavioural decisions and attentional competition in the prefrontal cortex. *Eur. J. Neurosci.* 56, 4393–4410.
44. Tang, H., Bartolo, R., and Averbeck, B.B. (2021). Reward-related choices determine information timing and flow across macaque lateral prefrontal cortex. *Nat. Commun.* 12, 894.
45. Kusunoki, M., Sigala, N., Nili, H., Gaffan, D., and Duncan, J. (2010). Target detection by opponent coding in monkey prefrontal cortex. *J. Cogn. Neurosci.* 22, 751–760.
46. Hampshire, A., Thompson, R., Duncan, J., and Owen, A.M. (2008). The target selective neural response—similarity, ambiguity, and learning effects. *PLoS One* 3, e2520.
47. Barak, O., Sussillo, D., Romo, R., Tsodyks, M., and Abbott, L.F. (2013). From fixed points to chaos: three models of delayed discrimination. *Prog. Neurobiol.* 103, 214–222.
48. Cole, M.W., and Schneider, W. (2007). The cognitive control network: integrated cortical regions with dissociable functions. *Neuroimage* 37, 343–360.
49. Duncan, J. (2010). The multiple-demand (MD) system of the primate brain: mental programs for intelligent behaviour. *Trends Cogn. Sci.* 14, 172–179.
50. Woolgar, A., Jackson, J., and Duncan, J. (2016). Coding of visual, auditory, rule, and response information in the brain: 10 years of multivoxel pattern analysis. *J. Cogn. Neurosci.* 28, 1433–1454.
51. Mitchell, D.J., Bell, A.H., Buckley, M.J., Mitchell, A.S., Sallet, J., and Duncan, J. (2016). A putative multiple-demand system in the macaque brain. *J. Neurosci.* 36, 8574–8585.
52. Benjamini, Y., and Hochberg, Y. (1995). Controlling the false discovery rate: A practical and powerful approach to multiple testing. *Journal of the Royal Statistical Society. Series B.* 57, 289–300.
53. Meyers, E.M. (2013). The neural decoding toolbox. *Front. Neuroinform.* 7, 8.
54. Oostenveld, R., Fries, P., Maris, E., and Schoffelen, J.M. (2011). FieldTrip: open source software for advanced analysis of MEG, EEG, and invasive electrophysiological data. *Comp. Intell. Neurosci.* 2011, 156869.

STAR★METHODS

KEY RESOURCES TABLE

REAGENT or RESOURCE	SOURCE	IDENTIFIER
Experimental models: Organisms/strains		
Rhesus monkeys	Centre for Macaques	N/A
Software and algorithms		
MATLAB Releases 2018a and 2020a	The MathWorks, Inc.	https://uk.mathworks.com/products/matlab.html
REX v 8	Laboratory of Sensorimotor Research, National Eye Institute, National Institutes of Health	https://datashare.nei.nih.gov/LsrDirectoryServlet
Neural Processing MATLAB Kit version 5.5.2.0	Blackrock Microsystems	https://github.com/BlackrockNeurotech/NPMK/
Neural decoding toolbox	Meyers et al. ⁵³	http://www.readout.info/toolbox-design/
FieldTrip	Oostenveld et al. ⁵⁴	https://www.fieldtriptoolbox.org/
GCMi version 0.4	Ince et al. ³³	https://github.com/robince/gcmi
Offline Sorter 3.3.5 and 4.6.2	Plexon Inc	https://plexon.com/products/offline-sorter/
Custom software	This paper	https://osf.io/v6w2h/

RESOURCE AVAILABILITY

Lead contact

Requests for further information and access to data should be directed to and will be fulfilled by the lead contact, John Duncan (john.duncan@mrc-cbu.cam.ac.uk).

Materials availability

This study did not generate new materials.

Data and code availability

- All data reported in this paper will be shared by the [lead contact](#) upon request.
- All original code has been deposited on OSF and is publicly available as of the date of publication. The DOI is listed in the [key resources table](#).
- Any additional information needed to reanalyse the data reported in this paper is available from the [lead contact](#) upon request.

EXPERIMENTAL MODEL AND SUBJECT DETAILS

Subjects were two male rhesus monkeys (*Macaca mulatta*), each weighing 14 kg. The experiments were performed in accordance with the Animals (Scientific Procedures) Act 1986 of the UK; all procedures were licensed by a Home Office Project License obtained after review by Oxford University's Animal Care and Ethical Review committee, and were in compliance with the guidelines of the European Community for the care and use of laboratory animals (EUV, European Union directive 86/609/EEC).

METHOD DETAILS

Task

Task events were controlled by REX real-time data acquisition and laboratory control software (developed by the National Institutes of Health), with displays presented on a 17.5 inch LED screen placed in front of the monkey's chair.

Animals were required to learn and select target objects for soft food reward. General features of the task, including instruction cues, stimulus arrays, saccadic responses, feedback signals and the structure of trials within each problem are described in the main text. On average animals completed 57 problems per session, all based on the same fixed set of eight objects (inset, [Figure 1A](#)).

Details of events on each trial are illustrated in [Figure 1A](#). Before the trial began, the screen showed a central white fixation point (FP) and a surrounding display of 6 black squares (each square 6 x 6 deg visual angle, centred 14 deg from fixation). To initiate trial events, the monkey was required to fix the eye on the FP (window 2.6 x 2.6 deg for animal A, 3 x 3 deg for animal B). At this point the FP turned red, and there was a wait period of 0.3 to 0.6 s, after which a cue stimulus appeared over the FP. The cue stimulus was also a 6 x 6 deg

square, grey in cycle 1, and green or yellow in cycles 2–4 when it indicated which of the problem's two targets to select. Following a delay of 0.5 or 1 s, fixed for each session, the circular array of black squares was replaced by an array of 6 choice objects. After a further delay of 1 to 2.5 s, the FP changed to cyan (GO) to indicate that a response could be made, and the cue stimulus disappeared. To indicate his choice, the animal made a saccade to one of the objects (saccade required within 1 s of GO). After fixation had been held on the selected object for 0.35 to 0.45 s, this object was replaced by a feedback signal (FB), a 6 × 6 deg square of either the original cue color (positive FB, target selected) or red (negative feedback, nontarget selected). This feedback remained for 0.4 s followed by an inter-trial display (see below). If the selected object was a target, a drop of soft food (reward, RW) was delivered 0.05 to 0.15 s after FB offset.

Once a trial had been initiated, it was aborted without reward if the monkey broke fixation prior to GO. The trial was also aborted if, after an object had been selected, fixation was not maintained until FB. Aborted trials were discarded before data analysis.

Different inter-trial displays indicated transitions within a cycle, between cycles, and between problems. For trials within a cycle, the inter-trial display was simply the white FP and surrounding black squares (see Figure 1A), with a minimum period of 0.7–0.9 s required before the next trial would begin. To indicate the end of a cycle, this display was preceded by a period of only the grey FP, lasting 3.2–3.5 s. To indicate the end of a problem, the screen blanked for 3.3–3.6 s.

Recordings

Each monkey was implanted with a titanium head holder and recording chambers (form fitting chamber system, Gray Matter Research), fixed on the skull with titanium or ceramic screws. Frontal chambers were placed over the lateral prefrontal cortex of the right hemisphere for both monkey A (target positions AP = 34.9, ML = 14.7; AP, anterior-posterior; ML, medio-lateral) and monkey B (AP = 36.4, ML = 19.1). Temporal chambers were placed over the parietal cortex of the right hemisphere for both monkey A (AP = 4.3, ML = 11.3) and monkey B (AP = 3.0, ML = 18.3). A craniotomy was made under each chamber for physiological recording. All surgical procedures were aseptic and carried out under general anaesthesia.

Recording locations for each animal are shown in Figure 1C. We used 96- and 32-channel semi-chronic microdrive systems respectively for the frontal and temporal chambers (SC-96 and SC-32, Gray Matter Research), with 1.5 mm inter-electrode spacing, interfaced to a multi-channel data acquisition system (Cerebus System, Blackrock Microsystems). Between sessions, to ensure recording of new cells, electrodes were advanced by a minimum of 62.5 μm. Neural activity was amplified, filtered (300 Hz to 10 kHz), and stored for offline cluster separation and analysis (Offline Sorter, Plexon). Eye position was sampled at 120 Hz using an infrared eye tracking system (Applied Science Laboratories) and stored for offline analysis. We did not preselect neurons for task-related responses; instead, we advanced microelectrodes until we could isolate neuronal activity before starting the task. Data were recorded over a total of 247 (122 with monkey A, 125 with B) daily sessions.

At the end of the experiments, animals were deeply anaesthetized with barbiturate and then perfused through the heart with heparinized saline followed by 10% formaldehyde in saline. The brains were removed for histology and recording locations confirmed (Figure 1C).

QUANTIFICATION AND STATISTICAL ANALYSIS

All statistical analyses were carried out using MATLAB (MathWorks).

For each cell, firing rates in each time window (see results) were examined by ANOVA to assess coding of object, location, and cue information. From each ANOVA we calculated proportion of explained variance (PEV) for each factor, and averaged this across all cells in each region. PEV was measured by the partial ω^2 index of effect size, calculated by the formula

$$\omega^2 = df_{\text{effect}} \times (MS_{\text{effect}} - MSE) / (SS_{\text{effect}} + (N_{\text{total}} - df_{\text{effect}}) \times MSE)$$

where df_{effect} is degrees of freedom for the factor of interest (object, location, cue), MS_{effect} is the mean square for the factor, SS_{effect} is the sum of squares for the factor, MSE is the mean square error, and N_{total} is the total number of observations (trials).

Within each region, randomization tests were used to assess the significance of mean PEV values across cells (Figures 2A, 6A, and 7A). For each neuron, labels (cue-object pairs for assessment of cue and object significance; locations for assessment of location significance) were randomized across trials, followed by re-calculation of mean PEV across cells. The PEV value for the true data was compared with the distribution obtained from 1000 repetitions of this randomization, and the p value determined by the proportion of randomized values greater than or equal to the true value. This procedure was repeated for each time window, and the criterion for significance was set at $p < .05$ corrected for multiple comparisons (time windows) by false discovery rate (FDR).⁵²

For comparison of PEVs between regions (Figures 6A, 7A, and S8), we used bootstrap resampling. For each of 1000 repetitions, we drew samples of cells from each region, matched in size to the original data but sampled with replacement. The p value was given by the proportion of samples with a mean difference between regions opposite to the majority, multiplied by 2 for a two-tailed test. Again the criterion for significance was set at $p < .05$ FDR corrected for multiple comparisons (time windows).

For temporal cross-generalisation analyses (Figures 2B, 6B, and 7B), MATLAB scripts and functions from the Neural Decoding toolbox⁵³ were modified as needed. Firing rates for each neuron were z scored normalized within the same 50 ms time windows used for ANOVA. Trials for each neuron were divided into k different splits, with $k - 1$ splits used to construct classifiers, and data from the remaining split used to test. A separate classifier was constructed for each time window in the train data, and its

classification accuracy measured for each window in the test data. We used a maximum correlation classifier. Each classifier consisted simply of C vectors of n mean firing rates from test data, where C is the number of classes and n is the number of neurons. Test data were pseudotrials, with each pseudo-trial constructed by selecting a single random trial from the test split of each neuron. For each pseudotrial, the test vector of n firing rates was correlated with the C vectors of the classifier, and assigned to the class with the highest correlation. This procedure was repeated k times, each time using a different held-out split, and then the entire process was repeated 100 times with different random splits, and the results averaged. For decoding of cue, object and location, k was set to 30, 10 and 7 respectively. Object decoding was measured separately for each of the two object sets, and the results averaged.

Again we used 1000 repetitions of label randomisation for statistical testing. For each repetition, we trained classifiers on true data, but for each neuron, randomised trial labels in the test data. Again, we randomised cue+object pairs for testing of cue and object decoding, and locations for testing of location decoding. After each randomisation of trial labels, we calculated a full decoding matrix. For each entry in the matrix, the p value was set to the proportion of randomized cases greater than the true value, and FDR corrected to a criterion of $<.05$ across the entire matrix.

For cross-validated testing of cue and object selectivity (Figure 3), data from each cell were normalized before calculating mean PSTHs across neurons. For each cell, normalization consisted of dividing mean spike rate in each time window by mean spike rate across the entire trial duration (-1 s from trial initiation to $+1$ s from feedback). For statistical testing we used paired t -tests across cells. Where the same cell was selected in both odd and even trial sets, results were averaged before entry into the t -test. We used a criterion of $p <.05$, FDR corrected across time windows.

For analyses of representational geometry (Figure 5), the mean spike rate of each recorded neuron was calculated for each condition (either the eight target objects, or the six target locations). From this neurons-by-conditions matrix, the pairwise Euclidean distance between conditions was calculated and submitted to classical multidimensional scaling (MDS, here equivalent to principal components analysis) to obtain a 2-dimensional embedding of the population response to each condition. 95% bootstrapped confidence ellipses were constructed by randomly resampling trials, with replacement, 1000 times; for each bootstrap sample, the MDS configuration was calculated in the same way, and aligned to the true configuration using Procrustes transformation. Procrustes transformation (without a scaling component) was also used to align configurations across time windows.

To test for flow of location information between vLPFC and dLPFC (Figure 8), we first selected sessions (16) from animal A that had at least 15 recorded neurons in each of vLPFC (mean 22.2 neurons recorded from mean 14.9 electrodes) and dLPFC (mean 24.5 neurons recorded from mean 17.0 electrodes). Animal B had no sessions that met this criterion. As input to the information flow analysis, we sought a continuously valued, moment-by-moment and trial-by-trial measure of location information per region. For this purpose, we used a Fisher linear discriminant classifier with diagonal covariance matrix and 5-fold cross-validation, per session, scoring location information per trial as the classifier's probability estimate of assigning the target location to the correct class (chance = $1/6$). All trials from cycles 2-4 with a correct response were included (mean 385.4 across sessions). To maximise sensitivity, the classifier was provided with both local firing rate per neuron and high frequency power (HFP) per electrode. To confirm that these features provided complementary information, the classifiers were also run with either firing rate or HFP alone. To estimate instantaneous HFP, the local field potential (LFP) was down-sampled to 1 kHz, notch-filtered at 50 Hz (and harmonics) and band-pass filtered between 70-250 Hz using the default options in Fieldtrip toolbox,⁵⁴ re-referenced to the average across electrodes per region, Hilbert-transformed, and squared. Within each epoch of interest (-200 to 1000 ms around array onset) occasional trials with artefactual spikes in the LFP were excluded if the notch-filtered LFP deviated from its mean by more than six standard deviations across the epoch (mean 12.8 trials in vLPFC and 19.0 trials in dLPFC). To estimate the local firing rate from the binary action potentials, and to account for variable timing of the HFP signal across trials, both the time-course of action potentials and instantaneous HFP were smoothed using a Gaussian kernel of 50 ms full-width-at-half-maximum (FWHM). Based on these smoothed data, continuous information time-courses were obtained by repeating decoding in 2 ms steps across the analysis epoch. Statistical significance of this location decoding analysis was assessed using a permutation test on the mean decoding performance, averaged across trials per target location, then across target locations, then across sessions. The null distribution was constructed from 1000 permutations, in which the target location labels were shuffled across trials per session. The criterion was set to $p <.05$, FDR-corrected across time points.

Having estimated per-trial time-courses of location information within each region, we quantified directed information flow (DI) between regions using the conditional mutual information (CMI) between the cross-trial vector of location information in the source region at time t and the target region at time $t + \text{lag}$, conditional on the target region at time t . This measure is an information theoretic analogue of Granger causality, and was estimated using the Gaussian-copula-based lower-bound proposed by Ince et al.^{32,33} Note that due to bias correction, CMI estimates can be negative, with an expectation of zero when there is no true relationship. To ensure trial-wise correspondence between the vectors, trials that had been marked bad in either region were excluded. DI was calculated in both directions (i.e. from vLPFC to dLPFC and vice-versa) across the whole epoch and across a range of lags (1-200 ms). Statistical significance was assessed using a permutation test on the mean DI across sessions. The null distribution was constructed from 1000 permutations, in which the source information was shuffled across trials per session. The criterion was set to $p <.05$, FDR-corrected across time points and lags.

For significance testing of cue index values (Figure S3), we again used a randomization approach. At each iteration, the sets of four objects assigned to the two cues were independently randomised for each neuron. The procedure was repeated 1000 times, and the p value was calculated as the proportion of randomised values greater than the true value. Again the criterion was set to $p <.05$, FDR corrected across time windows.